

Green Chemistry

Cutting-edge research for a greener sustainable future

Accepted Manuscript

View Article Online
View Journal

This article can be cited before page numbers have been issued, to do this please use: Z. Wang, Y. Qiu, Z. Cheng, H. Huang, Y. Sui, X. Liu, Y. Yang, Y. Lu, H. Zhu, Q. Ji and J. Yan, *Green Chem.*, 2025, DOI: 10.1039/D5GC02864G.



This is an Accepted Manuscript, which has been through the Royal Society of Chemistry peer review process and has been accepted for publication.

Accepted Manuscripts are published online shortly after acceptance, before technical editing, formatting and proof reading. Using this free service, authors can make their results available to the community, in citable form, before we publish the edited article. We will replace this Accepted Manuscript with the edited and formatted Advance Article as soon as it is available.

You can find more information about Accepted Manuscripts in the [Information for Authors](#).

Please note that technical editing may introduce minor changes to the text and/or graphics, which may alter content. The journal's standard [Terms & Conditions](#) and the [Ethical guidelines](#) still apply. In no event shall the Royal Society of Chemistry be held responsible for any errors or omissions in this Accepted Manuscript or any consequences arising from the use of any information it contains.

1. Our work transforms two major industrial waste streams (dimethyldivynylsilane and sulfur) into a high-value functional material using solvent-free inverse vulcanization.
2. We achieved atom-efficient conversion of low-value wastes into a dynamic polymer. Applied as a coating, it extends the lifespan of monolayer MoS₂ transistors as a candidate for next generation electronics by healing defects.
3. Further research will focus on low-energy, scalable synthesis, exploring diverse applications, and enabling closed-loop material recycling after end-of-life.

View Article Online
DOI: 10.1039/D5GC02864G



ARTICLE

Dynamic Sulfur-Rich Network from Silicone Industry Waste†

Zixiao Wang,^{‡a} Yuanyuan Qiu,^{‡a} Zheju Cheng,^a Honglu Huang,^a Yang Sui,^b Xin Liu,^a Yijie Yang,^{a,c} Yue Lu,^a Huie Zhu,^c Qingqing Ji^{*a} and Jiajun Yan^{*a}Received 00th January 20xx,
Accepted 00th January 20xx

DOI: 10.1039/x0xx00000x

Industrial waste accumulation poses significant environmental challenges. Dimethyldivinylsilane, a notable side product of the silicone industry is left without a specific use. Meanwhile, sulfur, the most common byproduct of the petrochemical industry, is frequently in surplus despite being largely utilized for sulfuric acid production. This study employed the inverse vulcanization technique to upcycle these two waste streams into sulfur-rich dynamic polymer networks. The silicon-based crosslinker contributed to distinct dynamic behaviors for the synthesized polymers compared to other inverse vulcanized networks, resulting in a variety of accessible morphologies dependent on specific processes. The produced sulfur-rich malleable film was found to enhance the high-temperature performance of monolayer MoS₂ transistors by healing the sulfur vacancies and suppressing the switching hysteresis. This investigation highlights the potential for industrial waste upcycling and its application in the future design of materials and devices.

Introduction

Recently, the emphasis on sustainable development has heightened the need for efficient recycling of industrial byproducts. In this context, two industrial wastes, dimethyldivinylsilane (DMDVS) and sulfur come into our view. DMDVS is an inevitable side-product in the production of 1,1,3,3-tetramethyl-1,3-divinylsiloxane (DVDSi) through the Wurtz-Fittig process (Fig. 1a).^{1–4} Silicon, the second most abundant element in the Earth's upper continental crust,⁵ underpins a well-developed silicon industry, in which DVDSi serves as a critical raw material; notably, it also serves as the ligand in Karstedt's catalyst for hydrosilylation, one of the largest-scale applications of homogeneous catalysis.^{6, 7} The global DVDSi production is consistently growing driven by continuous advancements in sectors such as coatings, adhesives, sealants, and electronic materials. However, at present, its side product DMDVS does not have any specific industrial application, resulting in a long-term storage and the risk of atmospheric release. On the other hand, sulfur, has a high abundance on Earth, making it the 16th most abundant in the Earth's upper continental crust,^{5, 8} predominantly occurring as sulfide and sulfate minerals, holds significant value in industry, agriculture, and materials science.^{9–11} Meanwhile, elemental sulfur today is mostly derived as a byproduct from the petrochemical industry during the sulfur removal processes

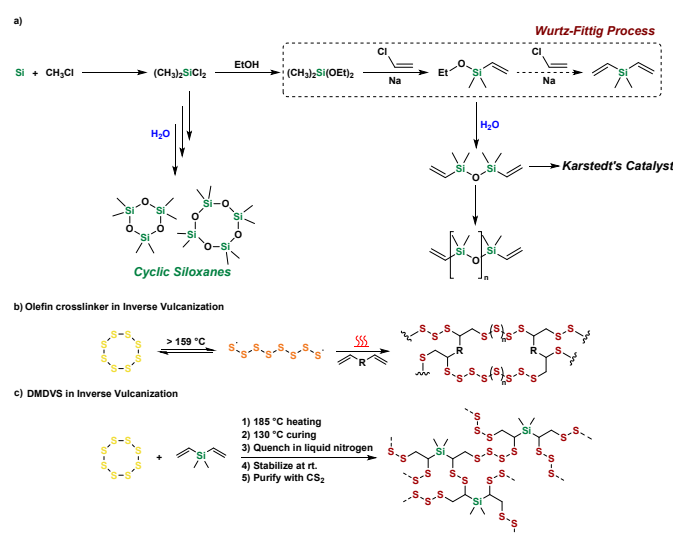


Fig. 1 Overview of DMDVS and its inverse vulcanization. (a) Production of siloxanes and DVDSi in silicone industry. (b) A general scheme of inverse vulcanization, where R indicates the core of small-molecule crosslinkers. (c) Proposed structure of poly(DMDVS-r-S) and key steps toward it.

from crude oil and natural gas.^{12, 13} Just in 2021 only, over 81 million tons of sulfur were produced across the globe,¹⁴ surpassing its consumption in sulfuric acid, fertilizers, and fungicides productions. The excess sulfur, stored as powder or bricks outdoors, presents potential environmental challenges that have yet to be fully addressed.^{8, 14–16}

Pyun and coworkers¹⁷ pioneered inverse vulcanization, a method to utilize these two abundant low-value chemicals. Inverse vulcanization is a solvent-free reaction that produces sulfur-rich functional polymer by radical polymerization between unsaturated organic crosslinkers and sulfur. Sulfur melts and undergoes ring-opening to produce chain-end radicals over 159 °C that add to crosslinkers (Fig. 1b).¹⁸ Since then, notable progress has been made in both the inverse

^aSchool of Physical Science and Technology, ShanghaiTech University, Shanghai 201210, P. R. China.

^bSchool of Life Science and Technology, ShanghaiTech University, Shanghai 201210, P. R. China.

^cZhangjiang Laboratory, Shanghai 201210, P. R. China

E-mail: jiqq@shanghaitech.edu.cn, yanjj@shanghaitech.edu.cn

† Electronic supplementary Information (ESI) available. See DOI:

‡ These authors contributed equally to this work.



vulcanization procedure and the applications of these unique sulfur-rich functional polymers. The range of organic crosslinkers explored for inverse vulcanization has expanded from synthetic feed-stocks, such as 1,3-diisopropenylbenzene^{17, 19, 20} and divinylbenzene,^{21, 22} to silicon-containing crosslinkers such as styrylethyltrimethoxysilane²³ and high-modulus reprobographic silicone,²⁴ to bio-based resources such as limonene,²⁵ vegetable oils,^{26, 27} thiocetic acid and its derivatives.^{28, 29} Presently, the primary methods for inverse vulcanization include heat activation,^{17, 30} diethyldithiocarbamate catalysis,³⁰ mechanochemical activation,³¹ chemical vapor deposition,^{32, 33} photo activation,³⁴ and anionic methods.^{35, 36} Beyond inverse vulcanization, several novel approaches for sulfur valorization have emerged. Pyun and co-workers have employed sulfonyl chlorides to synthesize disulfide-linked polymers.³⁷ Chalker and co-workers introduced trisulfide electrochemical and photochemical initiation strategies for the preparation of poly(trisulfide) materials.³⁸⁻⁴⁰ These sulfur-rich functional polymers can be utilized in various fields such as infrared optics,^{11, 19, 20, 40-44} antibacterial surfaces,⁴⁵⁻⁴⁸ pollution remediation,^{25, 31, 47, 49-51} precious metal acquisition,^{30, 39, 52} lithium-sulfur batteries,^{8, 11, 53-56} bitumen-like materials,⁵⁷ high-refractive-index coatings,^{32, 58} and pressure-sensitive adhesives.^{18, 28, 59, 60}

Herein, we report a new sulfur-rich dynamic polymer network produced by inverse vulcanization of DMDVS, effectively upcycling these low-value industrial side streams into an advanced functional material with unprecedented thermo-responsive behavior. Unlike conventional inversed vulcanized network, our polymer network exhibits unique dynamic behavior enabled by the distinctive molecular architecture of DMDVS, extended polysulfide domains stabilized by Si-based framework and temperature-dependent phase transitions. While being a viscous liquid at elevated temperature, it can be trapped in a gel state by rapid quenching. The network becomes instable at room temperature with spontaneous elemental sulfur segregation through a solid-solid transition. Upon removal of the elemental sulfur, it transforms into a denser yet fully reprocessable elastomer. Remarkably, the resulting sulfur-rich film serving as a packaging material, can improve the high-temperature performance of monolayer MoS₂ transistors by inhibiting sulfur vacancies in the latter.

Results and discussion

Material Preparation

Based on previous studies,^{57, 61-64} we establish an optimized procedure for DMDVS inverse vulcanization, consisting of five key steps as depicted in Fig. 1c: (1) 185 °C reaction, (2) curing at 130 °C, (3) liquid nitrogen quenching, (4) room-temperature stabilization, and (5) CS₂ (toxic !) extraction. As demonstrated in a prior work,¹⁷ effective inverse vulcanization requires homogeneously blending molten sulfur and a nonvolatile divinyl crosslinker at an elevated temperature to open S₈ rings and facilitate sulfur radical addition to vinyl groups.⁶⁵ However, DMDVS, with a low boiling point of 82 °C, is immiscible with

molten sulfur due to its rapid vaporization at > 100 °C. To overcome this challenge, we used a sealed tail-vial (Fig. S1) as a disposable reactor and condenser to house the reactants throughout the reaction.

The appearance of the mixture evolved throughout the reaction. It turned into a low viscosity orange liquid when initially heated to 185 °C, as shown in Fig. S2. After staying at 185 °C for 1 h, the system transformed into a pomegranate-red liquid with an increased viscosity. A curing step at 130 °C was implemented to allow thorough exchange and formation of the networks.⁶¹ After the temperature was maintained at 130 °C for 24 h, the system evolved into a dark red liquid with higher viscosity and became almost black for 45 h. As we quenched that dark viscous liquid in liquid nitrogen, it turned into a metastable elastic gel (Fig. S2a and Fig. S3), which sustained only below −5 °C (Fig. S4).

To distinguish the polymer networks prepared with different feeding ratios, we name them poly(DMDVS_x-r-S_y), where x and y are weight fractions of the two reactants in tenths. The gel obtained by rapid quenching is annotated poly(DMDVS_x-r-S_y)-G. The metastable gel slowly became a rusty brown solid at room temperature (Fig. 1c and Fig. S2a). The solid, annotated poly(DMDVS_x-r-S_y)-S (Fig. S3), was stable at room temperature. If the cured polymer melt was cooled slowly from 130 °C, it formed the same solid.

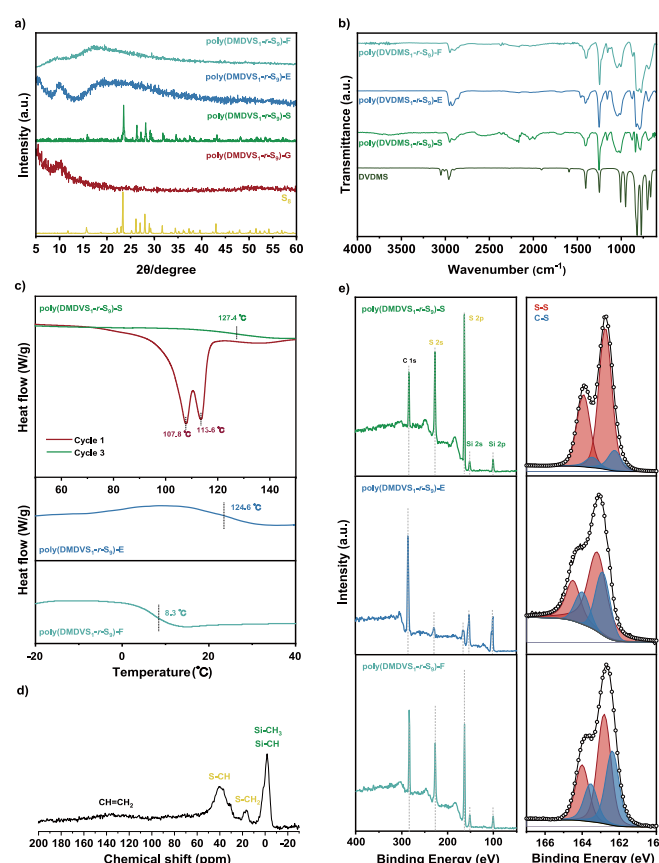


Fig. 2 Structural characterization of DMDVS-based inverse vulcanization polymers. (a) PXRD patterns of different poly(DMDVS₁-r-S₉) samples. (b) FT-IR spectra of poly(DMDVS₁-r-S₉) samples compared to DMDVS. (c) DSC curves. (d) ¹³C solid-state NMR of poly(DMDVS₁-r-S₉)-S. (e) Full XPS surveys and deconvoluting spectra of S 2p.



Table 1 Polymerization Conditions and Characteristics of Copolymers.View Article Online
DOI: 10.1039/D5GC02864G

Polymer ^a	$m_0(\text{DMDVS}) : m_0(\text{S}_8)$ (wt% : wt%)	Heating Time (h)	Curing Time (h)	Si Content ^b (wt%)	$T_{g, \text{DSC}}^c$ (°C)
Poly(DMDVS _{1.5-r-S_{8.5}})-S	15 : 85	1	45	0.669 ± 0.051	125.4
Poly(DMDVS _{1-r-S₉})-S	10 : 90	1	45	2.63 ± 0.21	127.4
Poly(DMDVS _{0.5-r-S_{9.5}})-S	5 : 95	1	45	0.440 ± 0.023	114.0
Poly(DMDVS _{1-r-S₉})-S	10 : 90	1	0	1.26 ± 0.35	134.2
Poly(DMDVS _{1-r-S₉})-S	10 : 90	1	24	2.21 ± 0.33	129.8
Poly(DMDVS _{1-r-S₉})-S	10 : 90	2	0	1.22 ± 0.13	134.2
Poly(DMDVS _{1-r-S₉})-S	10 : 90	2	24	1.91 ± 0.18	131.0
Poly(DMDVS _{1-r-S₉})-S	10 : 90	2	45	2.19 ± 0.23	124.8
Poly(DMDVS _{1-r-S₉})-S	10 : 90	3	0	1.15 ± 0.09	132.9
Poly(DMDVS _{1-r-S₉})-S	10 : 90	3	24	1.59 ± 0.18	128.8
Poly(DMDVS _{1-r-S₉})-S	10 : 90	3	45	1.70 ± 0.12	128.4

^a Reaction conditions: a 5 min quenching is set after curing. ^b Average weight ratio (wt %) of silicon is determined by ICP-OES in 4 parallel tests, errors are standard deviation of 4 samples and original data can be found in Table S1; ^c Extracted from the third cycle of DSC curves of each polymer. Full curves are available in Fig. S5.

As DMDVS is highly volatile at the reaction temperature, to exclude the possibility that what we observed was only the phase transition of sulfur,¹⁷ we recorded the appearance changes of elemental sulfur subjected to the same treatment (Fig. S2b). The molten sulfur was much lighter in color and the sample restored the original appearance as a yellow powder as it returned to room temperature. This validated that poly(DMDVS_{x-r-S_y}) is distinct from elemental sulfur while poly(DMDVS_{x-r-S_y})-S is its stable form. We also found that increasing DMDVS feeding inhibited polymerization. Poly(DMDVS_{2-r-S₈}) showed unexpected swelling prior to curing (Fig. S2c), indicating that the intended polymerization was inhibited. Therefore, a 10% DMDVS feeding was selected for further studies.

We examined the Si contents and glass transition temperatures (T_g) of these polymers prepared under different conditions (Table 1) by inductively coupled plasma optical emission spectrometer (ICP-OES) and differential scanning calorimetry (DSC) to preliminarily understand its composition. Interestingly, ICP-OES results revealed that poly(DMDVS_{1-r-S₉}) contained a greater Si content than samples with a smaller or larger DMDVS feeding. It was found that the silicon content has a negative correlation with reaction time but a positive correlation with curing time. Thus, the former contributed more to the evaporation as the latter helped with the incorporation.

As for the T_g , it has a negative correlation with curing time, indicating that curing promoted segment motion in the product, likely resulted from extended sulfur chains. The presence of a glass transition again proves that poly(DMDVS_{x-r-S_y}) is different from elemental sulfur which exhibited two endothermic peaks at 107.8 and 113.6 °C (Fig. 2c).⁶⁶ Taking these results into account, we selected poly(DMDVS_{1-r-S₉})-S from the second row with 1 h reaction of 45 h curing for the following studies.

Material Characterization

In an unexpected turn of events, our powder X-ray diffraction (PXRD) examination of the solids revealed a pattern of poly(DMDVS_{1-r-S₉})-S closely aligned with that of S₈ (Fig. 2a). This finding contradicted our earlier verdict that poly(DMDVS_{x-r-S_y}) differs from sulfur. Simultaneously, poly(DMDVS_{1-r-S₉})-G did not exhibit any discernible PXRD peak. This suggests that the sulfur signals in poly(DMDVS_{1-r-S₉})-S did not originate as a residue of the reactant. Instead, they were a result of transformations from poly(DMDVS_{1-r-S₉})-G when warmed to room temperature. Consequently, we postulate that a dynamic network with metastable long sulfur chains or rings were formed during the curing process, which were kinetically trapped by rapid quenching (Fig. 3a). As the temperature increased to ambient conditions, added thermal energy induced scission of the extended polysulfide chains, resulting in the formation of S₈ rings.

To verify that hypothesis, we first stored poly(DMDVS_{1-r-S₉})-G at -20 °C for over 6 months, observing no state change (Fig. S6). This proves the transformation toward poly(DMDVS_{1-r-S₉})-S does need a sufficient energy input. As described above, glass transition of poly(DMDVS_{x-r-S_y})-S was measured by DSC (Table 1 and Fig. S5) as evidence of its difference from sulfur. However, pairs of apparent endothermic peaks related to the elemental sulfur were observed only in the first DSC cycles of all poly(DMDVS_{x-r-S_y})-S samples. For poly(DMDVS_{x-r-S_y})-S samples without curing, a new melting peak slightly lower than the original pair was observed in the second DSC cycle, indicating a less crystalline species related to the reactant. During the subsequent cycles, only glass transitions were detectable (Fig. 2c and Fig. S5). This means that although elemental sulfur did exist in poly(DMDVS_{x-r-S_y})-S, the rate of its formation did not



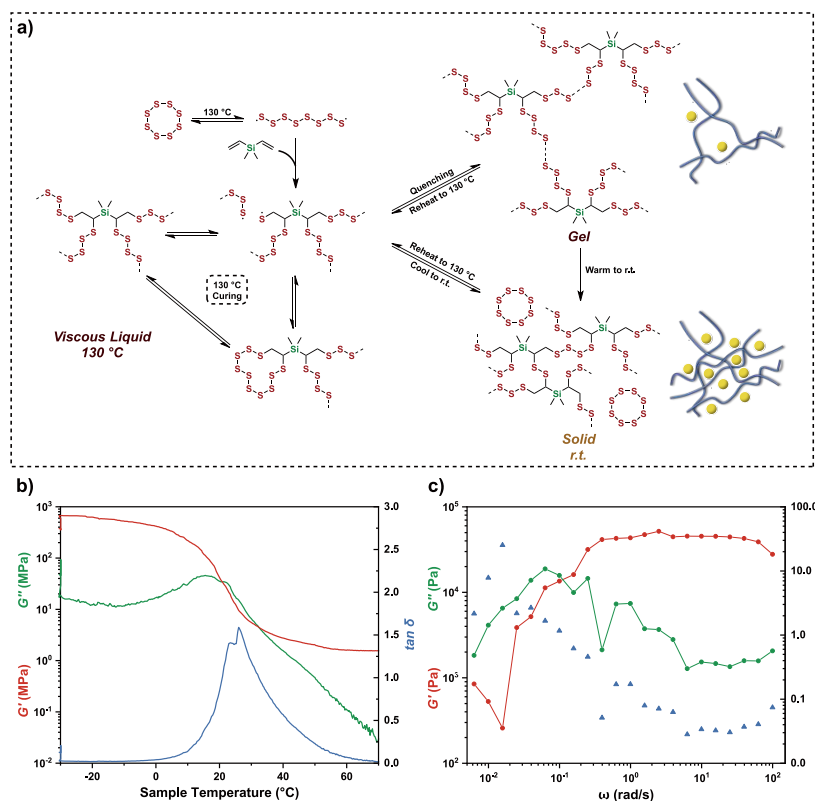


Fig. 3 Mechanical studies of poly(DMDVS_{1-r}-S₉)-G and proposed mechanisms. (a) The proposed mechanism of the reaction between DMDVS and S₈ and formation of different types of poly(DMDVS_{x-r}-S_y). (b) DMA of poly(DMDVS_{1-r}-S₉)-F. The specimen was cut into 8.0-mm × 35-mm × 0.10-mm (width × length × thickness). (c) Frequency sweep result of poly(DMDVS_{1-r}-S₉)-F sample at 150 °C and 0.2% strain.

keep pace with the fast 10 °C min⁻¹ heating/cooling in the ensuing cycles. Hence, the rapid heating/cooling in DSC essentially reversed the transformation from poly(DMDVS_{x-r}-S_y)-G to poly(DMDVS_{x-r}-S_y)-S. Based on these experiments, we can firmly conclude that poly(DMDVS_{x-r}-S_y)-S is a polymer network wherein S₈ originates from rearrangement of longer sulfur chains.

With that in mind, we tried to extract elemental sulfur and any soluble molecules from poly(DMDVS_{1-r}-S₉)-S (Fig. S7). However, all detected proton signals in the extracts were from the solvents implying the absence of soluble organic molecules. On the other hand, CS₂, with its exception ability to dissolve elemental sulfur, was able to remove all S₈ molecules to give a dark red elastomer, poly(DMDVS_{1-r}-S₉)-E (Fig. S3), as evidenced by the PXRD (Fig. 2a). Poly(DMDVS_{1-r}-S₉)-E had a slightly lower *T_g* (124.6 °C) than poly(DMDVS_{1-r}-S₉)-S (Fig. 2c), indicating similar segment mobility. Meanwhile, it no longer had sulfur melting peaks in the first cycle (Fig. S5). Without any structural information from the extracts, we instead turn to solid-state ¹³C nuclear magnetic resonance (NMR) and X-ray photoelectron spectroscopy (XPS) for an insight into the structure. We observed a sharp Si-C peak at ~ 0 ppm and a few broad S-C peaks from 10–60 ppm (Fig. 2d). Interestingly, a broad but weak vinyl bump at 130 ppm was also present. Poly(DMDVS_{1-r}-S₉)-E showed almost identical ¹³C NMR features (Fig. S8) but the Si-C peak split into two. This is likely a result of improved resolution after S₈ removal. We observed characteristic XPS peaks of S 2s, S 2p, Si 2s, and Si 2p in both poly(DMDVS_{1-r}-S₉)-S and poly(DMDVS_{1-r}-S₉)-E (Fig. 2e). The reduced intensity of sulfur

peaks in the full XPS surveys of poly(DMDVS_{1-r}-S₉)-E further confirmed the removal of crystalline sulfur. Assuming that each C=C bond formed two C-S bonds, we were able to determine the sulfur rank (SR)³³ of poly(DMDVS_{1-r}-S₉)-S base on Eq (1) that derived in Supporting Information and the silicon content measured by ICP-OES (Table 1).

$$SR = \frac{A_r(\text{Si}) - \omega_{\text{Si}} M_r(\text{DMDVS})}{2\omega_{\text{Si}} A_r(\text{S})} \quad (1)$$

where *A_r*(Si) and *A_r*(S) are the atomic mass of Si and S, *M_r*(DMDVS) is the molar mass of DMDVS and ω_{Si} is the Si content in Table 1, respectively.

This yield an SR of 14.9. Furthermore, by deconvoluting the S 2p doublets (Fig. 2e), we calculated an SR of 15.8 from Eq (2)³³ and Table S2, offering further consistency between the two methods.

$$SR = \frac{A_{\text{S-S}}}{A_{\text{C-S}}} \times 2 + 2 \quad (2)$$

where *A_{S-S}* and *A_{C-S}* are the areas of S-S and C-S signals in the deconvoluted S 2p doublet, respectively.

However, poly(DMDVS_{1-r}-S₉)-E does not digest fully even under high-temperature microwave treatment. We instead determined the SR to be 4.5 by deconvoluting S 2p doublets in high-resolution XPS scans (Fig. 2e)³³. These findings again verify our hypothesis on poly(DMDVS_{1-r}-S₉) transformations. Solubility tests further revealed that poly(DMDVS_{1-r}-S₉)-E had good resistance to common solvents (Fig. S9).

Fourier transform infrared (FT-IR) spectra (Fig. 2b) showed an absorption peak at 1157 cm⁻¹ corresponding to the C-S



stretching vibration in poly(DMDVS_{1-r}-S₉)-S and poly(DMDVS_{1-r}-S₉)-E, while the peaks related to -CH=CH₂ were absent. Peaks at 1406 cm⁻¹ and 1250 cm⁻¹ corresponding to Si-C bonds were still present in the polymer but with a shift in their intensity ratio from the DMDVS monomer. These observations mean that during the reaction, vinyl groups were mostly converted to C-S species albeit its detection by highly sensitive solid-state NMR acquisition. Meanwhile, the 400 cm⁻¹ S-S stretching were too weak to be observed^{18, 41, 64, 67}.

Due to a lack of stability, poly(DMDVS_{1-r}-S₉)-G is particularly difficult to characterize. We stored the sample in liquid nitrogen before performing the rheology test on it at -10 °C. The *G'* was slightly larger than *G''* over a range from 0.1 to 628.3 rad s⁻¹ (100 Hz), until a crossover at 421.6 rad s⁻¹ (67 Hz), while tan δ was nearly constant over a range from 0.1 to 23.7 rad s⁻¹, indicating a loose network with long sulfur chains between crosslinking points (Fig. S10a). Fig. S10b shows that poly(DMDVS_{1-r}-S₉)-G can sustain a small strain between the plates before breakage, when *G''* dropped below *G'* as the sulfur chains fractured.

Based on the results above, we conclude that the copolymerization process produces a temperature-responsive dynamic polymer network, poly(DMDVS_{x-r}-S_y). We propose a mechanism of the reaction between DMDVS and S₈, as illustrated in Fig. 3a. Initially, high temperature (185 °C) induces the cleavage of S-S in S₈ to generate sulfur radicals like other heat-activated inverse vulcanization processes^{17, 68, 69}. This is followed by bulk polymerization, leading to the formation of the sulfur-rich network with long sulfur chains or large sulfur rings. Rapid quenching in liquid nitrogen preserves these high-temperature structures, while low temperature (-20 °C, *e.g.*) storage kinetically traps the segment motion to retain this structure. At room temperature, the thermodynamically labile long sulfur chains undergo S-S bond cleavage and recombination to form a more stable short-chain network alongside S₈ interspersed in the network. Free S₈ can reintegrate into the polymer network by heating, as observed in DSC (Fig. 2c).

Our density functional theory (DFT) calculations by considering a simplified model of poly(DMDVS_{x-r}-S_y) further affirm the proposed mechanism, featuring a minimum at SR = 6 in the calculated energy landscape (Fig. S11 and Fig. S12), in agreement with the experimentally determined SR of poly(DMDVS_{1-r}-S₉)-E. It is anticipated that the DMDVS crosslinkers reduce the packing density of long sulfur chains, leading to prominent metastability in the high-SR case, while a moderate SR (*e.g.*, 4 – 6) achieves balance between ring tension and chain instability, contributing to the global formation energy minima. Such structural traits bestow the dynamic and temperature-responsive feature to the poly(DMDVS_{x-r}-S_y) material.

The random physical forms of as-prepared poly(DMDVS_{1-r}-S₉)-E brought challenges to subsequent studies. Meanwhile, the dynamic covalent characteristic makes this polymer reprocessable. Therefore, we hot-pressed poly(DMDVS_{1-r}-S₉)-E at 120 °C and 2 MPa for 3 min after a 3-min preheating. Poly(DMDVS_{1-r}-S₉)-E exhibited an excellent malleability (Fig. S13). We annotate the polymer film obtained over 3 hot-press

cycles poly(DMDVS_{1-r}-S₉)-F. The film had almost identical FT-IR spectrum as poly(DMDVS_{1-r}-S₉)-E but showed different PXRD patterns, glass transition temperature, and XPS (Fig. 2). Some lower angle features seen in poly(DMDVS_{1-r}-S₉)-E and poly(DMDVS_{1-r}-S₉)-G vanished after pressing, indicating a loss of long period orders, probably related to clusters. The glass transition temperature was over 100 °C lower while sulfur melting was still absent in the first cycle (Fig. S5). This significant decrease of *T_g* after hot-pressing suggested that the tight network in poly(DMDVS_{1-r}-S₉)-E rearranged into a loose network in poly(DMDVS_{1-r}-S₉)-F with the stress in network relaxed as suggested in earlier reports. Bischoff et al. classified inverse vulcanized polymers as covalent adaptable networks (CANs), which exhibit thermoset characteristics with exchangeable bonds²². The application of heat facilitates the exchange within CANs, altering their topology and rheological properties, thus enabling creep recovery and stress relaxation (Fig. S14). Rheological studies in previous work provide further evidence of active dynamic covalent process of S-S bonds in inverse vulcanized polymers over 100 °C^{22, 70}. The XPS showed stronger sulfur peaks indicating more sulfur presented at the surface, but there was only a subtle increase in SR to 4.9 (5.3 calculated from Eq (1) and Table S1), proving that the hot-press did not significantly alter the average length of sulfur chains.

We assessed the viscoelastic properties of the film by using dynamic mechanical analysis (DMA). Overall, the poly(DMDVS_{1-r}-S₉)-F film behaved as a lightly crosslinked elastomer. At lower temperature, its *G'* was larger than *G''*, and a glassy plateau with a *G'* close to 3 GPa was observed. The *G'* started to drop above 0 °C as the film entered its glass transition, followed by a rubbery plateau with a storage modulus of several MPa beyond 40 °C. The measured *T_g* (~ 25 °C) was higher than the DSC result (8.3 °C) (Fig. 3b). To investigate the high-temperature rheological behavior of poly(DMDVS_{1-r}-S₉)-F, we conducted rheological measurements at 150 °C. In the terminal region, *G''* exceeded the *G'* over a frequency range of 6.28 × 10⁻³ to 100 rad s⁻¹, with a crossover observed near 0.1 rad s⁻¹ (Fig. 3c). Comparative analysis of Fig. 3b and Fig. S10a reveals that both *G'* and *G''* values for poly(DMDVS_{1-r}-S₉)-F at -10 °C are greater than those of poly(DMDVS_{1-r}-S₉)-G. Meanwhile, poly(DMDVS_{1-r}-S₉)-G displayed a *G''* higher than its *G'*, while poly(DMDVS_{1-r}-S₉)-F exhibited *G''* exceeding *G'*. This suggested a denser network structure with shorter sulfur chain segments between crosslink points which was different from poly(DMDVS_{1-r}-S₉)-G formed in poly(DMDVS_{1-r}-S₉)-F. Rheological properties of these two samples were consistent with their morphologies.

The thermal processability and its room temperature glass transition behavior makes the poly(DMDVS_{1-r}-S₉)-F film suitable for solvent-free coating applications. The film demonstrated moderate hydrophobicity, as indicated by a water contact angle of 94.4° (Fig. S15). To assess its in-service stability, the sample was subjected to continuous heating at 150 °C, the highest operational temperature, in a nitrogen atmosphere, revealing a sustained sulfur release over 96 h, which was favorable filling the sulfur vacancies in the intended application (Fig. S16).

Material Application



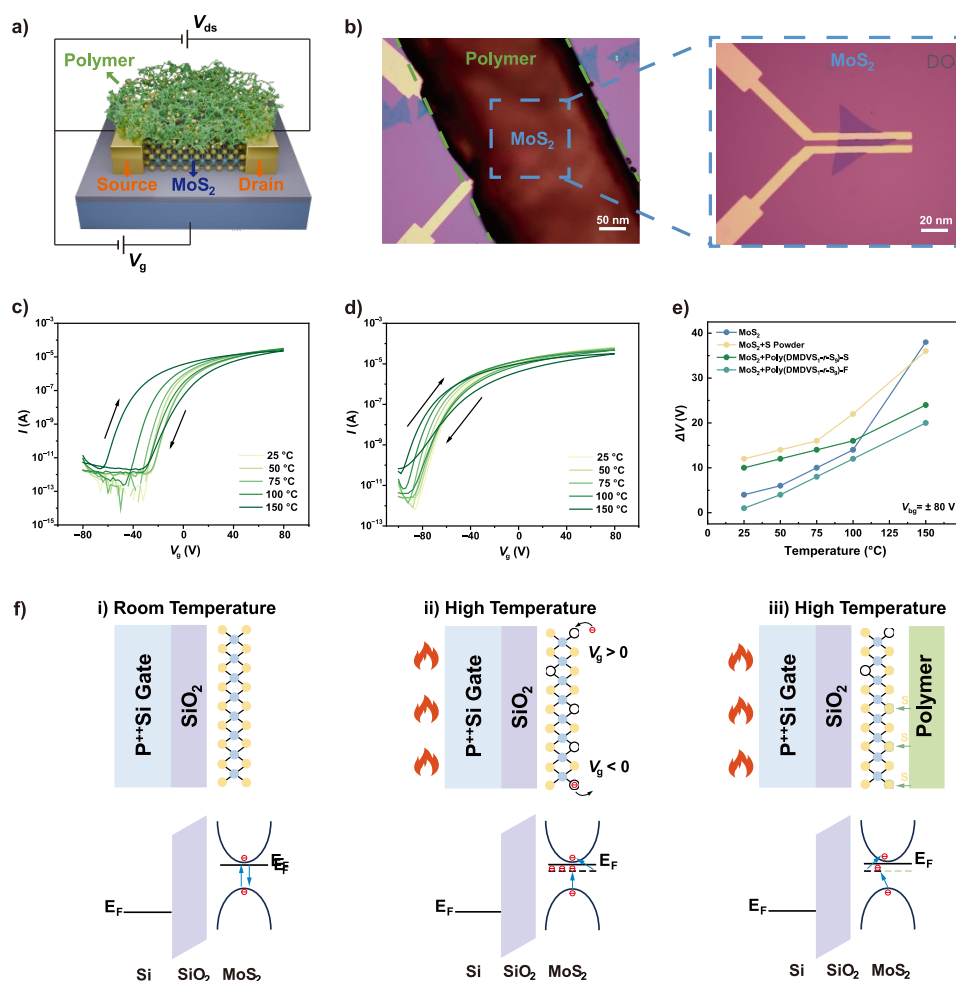


Fig. 4 Electrical characteristics of the MoS₂/poly(DMDVS_{1-r}-S₉)-F device. (a) Scheme and (b) optical micrograph of the MoS₂/poly(DMDVS_{1-r}-S₉)-F device. MoS₂ and poly(DMDVS_{1-r}-S₉)-F were outlined by the blue and green dashed line, respectively. Transfer curves of the MoS₂ FETs (c) without and (d) with poly(DMDVS_{1-r}-S₉)-F measured across varying temperatures in vacuum. V_g from -100 to 80 V back and forth at V_{ds} = 1 V. (e) Extracted hysteresis window as a function of temperature incorporating various sulfur-containing materials. (f) Proposed mechanisms for hysteresis alongside corresponding band diagrams: Thermally activated SVs act as electron trapping/de-trapping centers in MoS₂, whereas sulfur moieties in the polymer partially passivate these SVs, thereby suppressing the hysteresis window at elevated temperatures.

Two-dimensional (2D) materials, exemplified by graphene and monolayer MoS₂, have emerged as promising candidates for next-generation electronics due to their ultrathin bodies, dangling bond-free interfaces, and tunable band structures.⁷¹⁻⁷³ However, MoS₂-based devices face operational challenges under elevated temperature conditions. When exposed to temperatures approaching 100 °C, sulfur vacancies (SVs) in MoS₂ are thermally generated,^{74, 75} creating charge trapping centers.⁷⁶⁻⁷⁹ These SVs collectively degrade electrical stability, manifesting as both hysteresis window broadening and subthreshold swing (SS) degradation.⁸⁰

As illustrated in Fig. 4a and Fig. 4b, the polymer-encapsulated MoS₂ field-effect transistor (FET) architecture can effectively address this challenge. Fig. 4c and Fig. 4d display the transfer curves of MoS₂ and poly(DMDVS_{1-r}-S₉)-F/MoS₂ FETs, respectively, under cyclic V_{bg} sweep between -100 V and +80 V. For the bare MoS₂ device, the hysteresis window exhibits a substantial increase (Fig. 4c) from 4 V at 25 °C to 38 V at 150 °C. Poly(DMDVS_{1-r}-S₉)-F encapsulation effectively suppresses this thermally amplified hysteresis (Fig. 4d), reducing the hysteresis window from 38 V to 20 V. The suppression ratio, calculated by Eq (3) below, reaches 47% at 150 °C (Fig. 4e).

$$\text{Suppression Ratio} = \left(1 - \frac{\Delta V_{\text{polymer}}}{\Delta V_{\text{MoS}_2}}\right) \times 100\% \quad (3)$$

By contrast, the suppression ratios for sulfur powder and poly(DMDVS_{1-r}-S₉)-S are 5% and 36% (Fig. 4e and Fig. S17), respectively. This inefficiency arises from their side effects: physical adsorption of powders creates interface nonuniformity, which enlarge the baseline hysteresis even at room temperature (Fig. 4e).⁷⁶ Notably, poly(DMDVS_{1-r}-S₉)-F encapsulation does not induce additional hysteresis at 25 °C, confirming that its vacancy-passivating function is thermally activated and interface-protective. These results experimentally confirm the inhibitory effect of poly(DMDVS_{1-r}-S₉)-F on hysteresis window broadening of monolayer MoS₂ FETs at elevated temperatures.

In parallel with the hysteresis analysis, the temperature-dependent increase in SS exhibits a direct proportionality to SVs concentration ($\Delta SS \propto \Delta N_{\text{SVs}}$),^{81, 82} as derived in Supporting Information. To elucidate the quantitative relationship between sulfur vacancy concentration and SS degradation in MoS₂ FETs, we derived an analytical model based on semiconductor



electrostatics (Eq (S1) – Eq (S9)).⁸³ In this model, SS is expressed as a function of the depletion and oxide capacitances, with the depletion capacitance being influenced by the effective doping concentration (N_{eff}). Since thermally generated ΔN_{SVs} act as donor-like defects, they increase N_{eff} , leading to a measurable rise in SS. Assuming a proportional relationship between ΔN_{SVs} and ΔN_{eff} , we arrived at a simplified expression showing that ΔSS is directly proportional to ΔN_{SVs} . As summarized in Table S3, ΔSS at 150 °C is most severe in the bare MoS₂ FET (+2.22 V dec⁻¹, 84% SVs increase), corresponding to thermally activated sulfur volatilization. Poly(DMDVS_{1-r}-S₉)-F/MoS₂ FET shows a mitigated ΔSS of +0.99 V dec⁻¹ (21% SVs increase), validating its inhibitory effect against sulfur loss. Meanwhile, sulfur powder-coated and poly(DMDVS_{1-r}-S₉)-S-encapsulated FETs, exhibit intermediate SVs suppression (ΔN_{SVs} = 59% and 46%, respectively), limited by incomplete defect passivation due to insufficient interfacing. To describe the temperature-dependent charge trapping/de-trapping dynamics at the heterointerface, we have systematically constructed correlated hysteresis models accompanied by corresponding energy band diagrams (Fig. 4f).^{78, 79} At room temperature (25 °C), the hysteresis window in MoS₂ FET is nearly negligible in vacuum (Fig. 4c and Fig. 4e), confirming the intrinsically low SVs in pristine MoS₂ (Fig. S18).^{76, 77} Therefore, electrons are directly injected into the conduction band of MoS₂ under a positive gate voltage, whereas reversibly withdrawn under negative gate bias, resulting in a negligibly small hysteresis window, as shown in Fig. 4f-(i).

Under elevated temperature (e.g., 150 °C), sulfur atoms in the MoS₂ lattice acquire sufficient thermal energy to dissociate from their crystallographic positions, resulting in an increase in SVs.^{74, 75} These SVs introduce deep-level donor states below the conduction band edge (Fig. 4f-(ii)),⁷⁹ which act as dynamic charge trapping centers, resulting in pronounced hysteresis during gate voltage sweeps (Fig. 4c and Fig. 4e).⁷⁷ Under positive gate bias, electron trapping at vacancy sites increases the threshold voltage (V_{th}), whereas electron de-trapping under negative gate bias reduces V_{th} . This mechanism leads to a clockwise hysteresis in agreement with prior reports.^{76, 77}

Our experimental results have shown that the sulfur-rich poly(DMDVS_{1-r}-S₉)-F encapsulation layer undergoes thermally induced chain scission at elevated temperatures, releasing sulfur-containing moieties that coordinate with under-coordinated Mo atoms at the MoS₂ interface (Figure 4F-(iii)). This dynamic passivation process suppresses SVs formation below a critical threshold, stabilizing the hysteresis window and subthreshold swing. This approach hence unlocks the application potential of two-dimensional sulfide materials in high-temperature electronics, harnessing the sustained sulfur release property of the dynamic sulfur-rich network.

Conclusions

In summary, this work has demonstrated a waste-to-value transformation of sulfur-rich dynamic polymer networks from the combination of two considerable forms of industrial waste: dimethyldivinylsilane and elemental sulfur. Elevated temperatures prompt the S₈ ring to open, resulting in radical

polymerization in a viscous fluid that solidifies upon cooling, forming an elastic gel when the liquid mixture is rapidly quenched in liquid nitrogen and stored at low temperatures. Warming this gel triggers decomposition that leaves behind elemental sulfur and a denser network. Following the removal of such elemental sulfur, the residual sulfur-rich network can be molded into films, showing potential as a protective coating for monolayer MoS₂ transistors. This coating as a sulfur reservoir significantly reduces the switching hysteresis of the device by 47% at 150 °C, thanks to the sustained sulfur release of the polymer that passivate the otherwise abundant sulfur vacancies in MoS₂. The inherent dual-vinyl functionalities of dimethyldivinylsilane endow it with immense potential in constructing functional polymers. This work plants the seed of possibility in transforming low-value industrial waste into functional materials for future advancements, thereby advocating for an increased focus on the value-added applications of waste chemicals. We envision this study opening another path towards achieving sustainability.

Author contributions

Conceptualization, J.Y., Q.J., and Z.W.; methodology, Z.W., J.Y., Q.J., Y.L., and Y.Q.; validation, J.Y., Q.J., and Z.W.; formal analysis, Z.W., J.Y., Y.Q., and Q.J.; investigation, Z.W., Y.Q., Z.C., H.H., Y.S., X.L., Y.Y., and Y.L.; resources, J.Y. and Q.J.; data curation, Z.W., Y.Q., J.Y., and Q.J.; writing – original draft, Z.W., J.Y., and Y.Q.; writing – review & editing, J.Y. and Q.J.; visualization, Z.W., Y.Q., and Y.S.; supervision, J.Y., Q.J., and H.Z.; project administration, J.Y., Q.J., and H.Z.; funding acquisition, J.Y., Q.J., H.Z., and H.H.

Conflicts of interest

Part of the results have been filed in a pending patent application (CN118930861A) by ShanghaiTech University with J.Y., Z.W., and Z.C. as inventors. Zhejiang Jiancheng New Materials Co., Ltd, a material donor, may potentially benefit from the findings.

Data availability

The data supporting the findings of this study are available from the corresponding author upon reasonable request. All experimental data, including experimental methods, raw measurements, characterization results and calculations have been included in ESI.†

Acknowledgements

This work is financially supported by ShanghaiTech University via the start-up grant (J.Y.) and the Double First-Class Initiative Fund (H.H.), the Science and Technology Commission of Shanghai Municipality via Grant No. 22YF1428200 (J.Y.), and the National Natural Science Foundation of China via Grant No. 22401188 (J.Y.) and 22205142 (Q.J.). We thank Zhejiang



Jiancheng New Materials Co., Ltd for their kind donation of dimethyldivinylsilane. We thank Prof. Yingbo Zhao for the access to the DMA and Prof. Yijun Zheng for the access to the rheometer. We also thank the support from Analytical Instrumentation Center (Contract No. SPST-AIC10112914) at School of Physical Science and Technology, ShanghaiTech University.

References

- W. C. Schumb, J. Ackerman, Jr. and C. M. Saffer, Jr., *J. Am. Chem. Soc.*, 1938, **60**, 2486-2488.
- M. Kanazashi, *Bull. Chem. Soc. Jpn.*, 1953, **26**, 493-496.
- China Pat.*, CN101792459, 2010.
- China Pat.*, CN112625058, 2021.
- A. A. Yaroshevsky, *Geochem. Int.*, 2006, **44**, 48-55.
- A. M. Tondreau, C. C. H. Atienza, K. J. Weller, S. A. Nye, K. M. Lewis, J. G. P. Delis and P. J. Chirik, *Science*, 2012, **335**, 567-570.
- T. K. Meister, K. Riener, P. Gigler, J. Stohrer, W. A. Herrmann and F. E. Kühn, *ACS Catal.*, 2016, **6**, 1274-1284.
- J. J. Griebel, R. S. Glass, K. Char and J. Pyun, *Prog. Polym. Sci.*, 2016, **58**, 90-125.
- D. A. Boyd, *Angew. Chem., Int. Ed.*, 2016, **55**, 15486-15502.
- Y. Zhang, R. S. Glass, K. Char and J. Pyun, *Polym. Chem.*, 2019, **10**, 4078-4105.
- T. Lee, P. T. Dirlam, J. T. Njardarson, R. S. Glass and J. Pyun, *J. Am. Chem. Soc.*, 2022, **144**, 5-22.
- R. J. Angelici, *Acc. Chem. Res.*, 1988, **21**, 387-394.
- T. Rauchfuss, *Nat. Chem.*, 2011, **3**, 648-648.
- C. King-Poole and H. Thérien-Aubin, *Adv. Funct. Mater.*, 2024, **34**, 2405608.
- J. Lim, J. Pyun and K. Char, *Angew. Chem., Int. Ed.*, 2015, **54**, 3249-3258.
- T. Tian, R. Hu and B. Z. Tang, *J. Am. Chem. Soc.*, 2018, **140**, 6156-6163.
- W. J. Chung, J. J. Griebel, E. T. Kim, H. Yoon, A. G. Simmonds, H. J. Ji, P. T. Dirlam, R. S. Glass, J. J. Wie, N. A. Nguyen, B. W. Guralnick, J. Park, Á. Somogyi, P. Theato, M. E. Mackay, Y.-E. Sung, K. Char and J. Pyun, *Nat. Chem.*, 2013, **5**, 518-524.
- J. Fan, C. Ju, S. Fan, X. Li, Z. Zhang and N. Hadjichristidis, *Angew. Chem., Int. Ed.*, 2025, **64**, e202418764.
- J. J. Griebel, N. A. Nguyen, S. Namnabat, L. E. Anderson, R. S. Glass, R. A. Norwood, M. E. Mackay, K. Char and J. Pyun, *ACS Macro Lett.*, 2015, **4**, 862-866.
- T. S. Kleine, N. A. Nguyen, L. E. Anderson, S. Namnabat, E. A. LaVilla, S. A. Showghi, P. T. Dirlam, C. B. Arrington, M. S. Manchester, J. Schwiegerling, R. S. Glass, K. Char, R. A. Norwood, M. E. Mackay and J. Pyun, *ACS Macro Lett.*, 2016, **5**, 1152-1156.
- S. Diez, A. Hoeffling, P. Theato and W. Pauer, *Polymers*, 2017, **9**.
- D. J. Bischoff, T. Lee, K.-S. Kang, J. Molineux, W. O'Neil Parker, J. Pyun and M. E. Mackay, *Nat. Commun.*, 2023, **14**, 7553.
- J. M. Scheiger, C. Direksilp, P. Falkenstein, A. Welle, M. Koenig, S. Heissler, J. Matysik, P. A. Levkin and P. Theato, *Angew. Chem., Int. Ed.*, 2020, **59**, 18639-18645.
- M. Rokni, K. W. Park, W. Ho Leung, Z. Zujovic and E. M. Leitao, *Mater. Adv.*, 2024, **5**, 5433-5441.
- M. P. Crockett, A. M. Evans, M. J. H. Worthington, I. S. Albuquerque, A. D. Slattery, C. T. Gibson, J. A. Campbell, D. A. Lewis, G. J. L. Bernardes and J. M. Chalker, *Angew. Chem., Int. Ed.*, 2016, **55**, 1714-1718.
- J. Cubero-Cardoso, A. A. Cuadri, F. G. Feroso, J. E. Martín-Alfonso and J. Urbano, *ACS Appl. Polym. Mater.*, 2022, **4**, 3667-3675.
- A. Hoeffling, Y. J. Lee and P. Theato, *Macromol. Chem. Phys.*, 2017, **218**, 1600303.
- Y. Deng, Z. Huang, B. L. Feringa, H. Tian, Q. Zhang and D.-H. Qu, *Nat. Commun.*, 2024, **15**, 3855.
- C.-Y. Shi, X.-P. Zhang, Q. Zhang, M. Chen, H. Tian and D.-H. Qu, *Chem. Sci.*, 2024, **15**, 17460-17468.
- X. Wu, J. A. Smith, S. Petcher, B. Zhang, D. J. Parker, J. M. Griffin and T. Hasell, *Nat. Commun.*, 2019, **10**, 647.
- P. Yan, W. Zhao, F. McBride, D. Cai, J. Dale, V. Hanna and T. Hasell, *Nat. Commun.*, 2022, **13**, 4824.
- D. H. Kim, W. Jang, K. Choi, J. S. Choi, J. Pyun, J. Lim, K. Char and S. G. Im, *Sci. Adv.*, 2020, **6**, eabb5320.
- K. Choi, W. Jang, W. Lee, J. S. Choi, M. Kang, J. Kim, K. Char, J. Lim and S. G. Im, *Macromolecules*, 2022, **55**, 7222-7231.
- J. Jia, J. Liu, Z.-Q. Wang, T. Liu, P. Yan, X.-Q. Gong, C. Zhao, L. Chen, C. Miao, W. Zhao, S. Cai, X.-C. Wang, A. I. Cooper, X. Wu, T. Hasell and Z.-J. Quan, *Nat. Chem.*, 2022, **14**, 1249-1257.
- H. Yang, J. Huang, Y. Song, H. Yao, W. Huang, X. Xue, L. Jiang, Q. Jiang, B. Jiang and G. Zhang, *J. Am. Chem. Soc.*, 2023, **145**, 14539-14547.
- H. Yang, J. Zhang, W. Huang and G. Zhang, *Angew. Chem., Int. Ed.*, 2025, **64**, e202414244.
- K.-S. Kang, C. Olikagu, T. Lee, J. Bao, J. Molineux, L. N. Holmen, K. P. Martin, K.-J. Kim, K. H. Kim, J. Bang, V. K. Kumirov, R. S. Glass, R. A. Norwood, J. T. Njardarson and J. Pyun, *J. Am. Chem. Soc.*, 2022, **144**, 23044-23052.
- J. M. M. Pople, T. P. Nicholls, L. N. Pham, W. M. Bloch, L. S. Lisboa, M. V. Perkins, C. T. Gibson, M. L. Coote, Z. Jia and J. M. Chalker, *J. Am. Chem. Soc.*, 2023, **145**, 11798-11810.
- M. Mann, T. P. Nicholls, H. D. Patel, L. S. Lisboa, J. M. M. Pople, L. N. Pham, M. J. H. Worthington, M. R. Smith, Y. Yin, G. G. Andersson, C. T. Gibson, L. J. Esdaile, C. E. Lenehan, M. L. Coote, Z. Jia and J. M. Chalker, *Nat. Sustain.*, 2025.
- S. J. Tokin, H. D. Patel and J. M. Chalker, *ChemRxiv*, 2025, preprint, DOI: 10.26434/chemrxiv-2025-wd224-v2.
- J. J. Griebel, S. Namnabat, E. T. Kim, R. Himmelhuber, D. H. Moronta, W. J. Chung, A. G. Simmonds, K.-J. Kim, J. van der Laan, N. A. Nguyen, E. L. Dereniak, M. E. Mackay, K. Char, R. S. Glass, R. A. Norwood and J. Pyun, *Adv. Mater.*, 2014, **26**, 3014-3018.
- Y. Wuliu, W. Dong, G. Huang, H. Xie, P. Yao, J. Tan, K. Mu, Z. Zhang, Y. Chen, M. Wang, L. Tian, C. Zhu and J. Xu, *Angew. Chem., Int. Ed.*, 2025, **64**, e202419446.
- J. Pyun and R. A. Norwood, *Prog. Polym. Sci.*, 2024, **156**, 101865.
- J. Molineux, T. Lee, K. J. Kim, K.-S. Kang, N. P. Lyons, A. Nishant, T. S. Kleine, S. W. Durfee, J. Pyun and R. A. Norwood, *Adv. Opt. Mater.*, 2024, **12**, 2301971.
- Z. Deng, A. Hoeffling, P. Théato and K. Lienkamp, *Macromol. Chem. Phys.*, 2018, **219**, 1700497.
- R. A. Dop, D. R. Neill and T. Hasell, *Biomacromolecules*, 2021, **22**, 5223-5233.
- X. Deng, R. A. Dop, D. Cai, D. R. Neill and T. Hasell, *Adv. Funct. Mater.*, 2024, **34**, 2311647.
- S. K. Wijeyatunga, P. Y. Saucedo-Oloño, N. L. Kapuge Dona, B. G. S. Guinati, K. M. Derr, K. A. Tisdale, A. D. Smith, A. G. Tennyson and R. C. Smith, *Molecules*, 2025, **30**, 1614.
- T. Hasell, D. J. Parker, H. A. Jones, T. McAllister and S. M. Howdle, *Chem. Commun.*, 2016, **52**, 5383-5386.
- M. J. H. Worthington, R. L. Kucera and J. M. Chalker, *Green Chem.*, 2017, **19**, 2748-2761.
- D. J. Parker, S. T. Chong and T. Hasell, *RSC Adv.*, 2018, **8**, 27892-27899.
- J. Rollins, C. B. Call, D. Herrera and C. L. Jenkins, *ACS Appl. Polym. Mater.*, 2025, **7**, 8529-8537.



- 53 A. G. Simmonds, J. J. Griebel, J. Park, K. R. Kim, W. J. Chung, V. P. Oleshko, J. Kim, E. T. Kim, R. S. Glass, C. L. Soles, Y.-E. Sung, K. Char and J. Pyun, *ACS Macro Lett.*, 2014, **3**, 229-232.
- 54 J. W. Choi and D. Aurbach, *Nat. Rev. Mater.*, 2016, **1**, 16013.
- 55 L. Zhao, F. Qiu, X. Deng, Y. Huang, Y. Li, C. Zhao, W. Ren, C. Zou, X. Li, M. Wang and Y. Lin, *ACS Appl. Energy Mater.*, 2022, **5**, 7617-7626.
- 56 M. Wang, Z. Bai, T. Yang, C. Nie, X. Xu, Y. Wang, J. Yang, S. Dou and N. Wang, *Adv. Energy Mater.*, 2022, **12**, 2201585.
- 57 K.-X. Hou, P.-C. Zhao, L. Duan, M. Fan, P. Zheng and C.-H. Li, *Adv. Funct. Mater.*, 2023, **33**, 2306886.
- 58 X. Qian, *ACS Omega*, 2025, **10**, 3953-3959.
- 59 C. Herrera, K. J. Ysinga and C. L. Jenkins, *ACS Appl. Mater. Interfaces*, 2019, **11**, 35312-35318.
- 60 S. J. Tonkin, C. T. Gibson, J. A. Campbell, D. A. Lewis, A. Karton, T. Hasell and J. M. Chalker, *Chem. Sci.*, 2020, **11**, 5537-5546.
- 61 N. Han, W. Cho, J. H. Hwang, S. Won, D.-G. Kim and J. J. Wie, *Polym. Chem.*, 2023, **14**, 943-951.
- 62 B. Zheng, L. Zhong, X. Wang, P. Lin, Z. Yang, T. Bai, H. Shen and H. Zhang, *Nat. Commun.*, 2024, **15**, 5507.
- 63 T. Sehn, J. Fanelli, L. Wahl and M. A. R. Meier, *RSC Sustainability*, 2025, **3**, 291-299.
- 64 M. Vera-Tuset, R. Mas-Ballesté, I. Cuadrado, A. Moya and S. Bruña, *Polym. Chem.*, 2024, **15**, 1015-1025.
- 65 V. B. Purohit, M. Pięta, J. Pietrasik and C. M. Plummer, *Polym. Chem.*, 2022, **13**, 4858-4878.
- 66 L. Zhang, Y. Ren, X. Liu, F. Han, K. Evans-Lutterodt, H. Wang, Y. He, J. Wang, Y. Zhao and W. Yang, *Sci. Rep.*, 2018, **8**, 4558.
- 67 K. W. Park, E. A. Tafil, F. Fan, Z. Zujovic and E. M. Leitao, *Polym. Chem.*, 2022, **13**, 4717-4726.
- 68 R. S. Glass, in *Sulfur Chemistry*, ed. X. Jiang, Springer International Publishing, Gewerbestrasse, Cham, Switzerland, 2019, ch. 10, pp. 325-366.
- 69 B. Meyer, *Chem. Rev.*, 1976, **76**, 367-388.
- 70 J. J. Griebel, N. A. Nguyen, A. V. Astashkin, R. S. Glass, M. E. Mackay, K. Char and J. Pyun, *ACS Macro Lett.*, 2014, **3**, 1258-1261.
- 71 Y. Yoon, K. Ganapathi and S. Salahuddin, *Nano Lett.*, 2011, **11**, 3768-3773.
- 72 Q. H. Wang, K. Kalantar-Zadeh, A. Kis, J. N. Coleman and M. S. Strano, *Nat. Nanotechnol.*, 2012, **7**, 699-712.
- 73 H. Wang, L. Yu, Y.-H. Lee, Y. Shi, A. Hsu, M. L. Chin, L.-J. Li, M. Dubey, J. Kong and T. Palacios, *Nano Lett.*, 2012, **12**, 4674-4680.
- 74 H. Qiu, L. Pan, Z. Yao, J. Li, Y. Shi and X. Wang, *Appl. Phys. Lett.*, 2012, **100**.
- 75 S. Tongay, J. Suh, C. Ataca, W. Fan, A. Luce, J. S. Kang, J. Liu, C. Ko, R. Raghunathanan, J. Zhou, F. Ogletree, J. Li, J. C. Grossman and J. Wu, *Sci. Rep.*, 2013, **3**, 2657.
- 76 D. J. Late, B. Liu, H. S. S. R. Matte, V. P. Dravid and C. N. R. Rao, *ACS Nano*, 2012, **6**, 5635-5641.
- 77 N. Kaushik, D. M. A. Mackenzie, K. Thakar, N. Goyal, B. Mukherjee, P. Boggild, D. H. Petersen and S. Lodha, *npj 2D Mater. Appl.*, 2017, **1**, 34.
- 78 J. Kim, B. Seo, S. H. Lee, S. W. Jeong and Y. Roh, *J. Nanosci. Nanotechnol.*, 2017, **17**, 7327-7330.
- 79 M. Gu, T. Kim, D. Jeon, D. Lee, J. Park and T. Kim, *ACS Appl. Electron. Mater.*, 2024, **6**, 8525-8531.
- 80 Z. Hu, Z. Wu, C. Han, J. He, Z. Ni and W. Chen, *Chem. Soc. Rev.*, 2018, **47**, 3100-3128.
- 81 W. Zhu, T. Low, Y.-H. Lee, H. Wang, D. B. Farmer, J. Kong, F. Xia and P. Avouris, *Nat. Commun.*, 2014, **5**, 3087.
- 82 H. Jung, M. Kim, Y. Lee, G. B. Sim, H. Gu, S. Hong, S. Lee, J. Lee, D. Lee, T. Zou, K. Kang, C. W. Myung, Y.-Y. Noh and J. Kwon, *ACS Nano*, 2025, **19**, 6069-6078.
- 83 S. M. Sze and K. K. Ng, in *Physics of Semiconductor Devices*, eds. S. M. Sze and K. K. Ng, John Wiley & Sons, Inc., Hoboken, NJ, USA, 3 edn., 2006, ch. 6, pp. 293-373.



Data availability

The data supporting the findings of this study are available from the corresponding author upon reasonable request. All experimental data, including experimental methods, raw measurements, characterization results and calculations have been included in ESI.†

